Engineering a microfluidic platform for cell extravasation monitoring and downstream characterization of disseminated cells

Aude Sivery, Flavie Woesteland, Jérémy Duval, Marie Denoulet, Fabrice Soncin, Xuefen Le Bourhis, Anthony Treizebré, Chann Lagadec

Engineering a microfluidic platform for cell extravasation monitoring and downstream characterisation of disseminated cells

Aude Sivéry[a‡], Flavie Woesteland[b‡], Jérémy Duval[b], Marie Denoulet[b], Fabrice Soncin[c,d], Xuefen Le Bourhis[b], and Anthony Treizebre[a,c•], Chann Lagadec[b,c•]

[a]Univ. Lille, CNRS, Univ Polytechnique Hauts-de-France, Junia, UMR 8520 - IEMN – Institut d'Electronique de Microélectronique et de Nanotechnologie, F-59000 Lille, France
[b]UMR9020—U1277-CANTHER—Cancer Heterogeneity, Plasticity and Resistance to Therapies, University of Lille, CNRS, Inserm, CHU Lille, F-59000 Lille, France
[c]CNRS/IIS/Centre Oscar Lambret/Lille University SMMiL-E Project, CNRS Délégation Hauts-de-France, 43 Avenue le Corbusier, 59800 Lille, France.
[d]CNRS, IRL2820, Laboratory for Integrated Micro Mechatronic Systems, Institute of Industrial Science, University of Tokyo, 4-6-1 Komaba, Meguro-ku, Tokyo 153-8505, Japan

Correspondence to: chann.lagadec@inserm.fr; anthony.treizebre@univ-lille.fr

‡ These authors contributed equally to this work as co-first authors
• These authors contributed equally to this work as co-last authors

Metastatic cancer cells and immune cells spread throughout the body via the bloodstream, reaching target sites for immune clearance or establishing secondary tumors in distant organs. As they move from blood circulation to a targeted organ, cells adhere to activated endothelium and then extravasate through it into a tissue-rich environment. The molecular mechanisms that drive the extravasation of immune and cancer cells are not yet fully understood. Most importantly, the phenotypic state identity of the disseminated cancer cells has yet to be characterized. While various sealed microfluidic devices have been developed to study extravasation, few, if any, allow for the efficient collection of extravasated cells. To address this limitation, we designed a biomimetic microfluidic device comprising a network of 3D blood capillaries and a customizable collecting chamber, separated by a porous membrane. Our device enables i) real-time monitoring of cell extravasation through the endothelium via live imaging and ii) the collection of disseminated cells for subsequent molecular characterization. We validated the functional properties of the 3D endothelial layer under shear stress and inflammation induction. After injecting promyeloblast cells and metastatic cancer cells into the lumen of the capillary network, we observed cell rolling and extravasation under continuous flow conditions. Finally, we collected extravasated cancer cells for gene expression profiling by RT-qPCR. Overall, our novel microfluidic device reconstitutes a functional 3D blood vessel network, allowing real-time observation of extravasation and the collection of disseminated cells for further characterization.

Keywords: Microfluidic device, Extravasation process, Metastasis, Breast Cancer

Introduction

Metastasis is responsible for most cancer-related deaths. It involves cancer cells acquiring traits that enable them to escape from the primary tumor, spread, intermittently enter and exit dormancy, and establish colonies in distant organs (1). These processes are governed by clonal selection, the ability to transition between distinct states, and immune system evasion (2). Yet our knowledge of this process as a dynamic, heterogeneous, and systemic disease—and how to treat it effectively—remains limited.

Metastasis occurs when cancer cells detach from the primary tumor, travel in the lymph or blood vessels, and reach a specific tissue or organ to establish a secondary tumor (3). During this process, cells must perform sequential events, including invasion of surrounding tissues, intravasation through the blood vessels into the bloodstream, survival in the circulation, extravasation, establishment, and proliferation at a secondary site in a novel environment (4). A very small fraction of cancer cells (between 0.001 and 0.02%) that enter the circulation can potentially create a malignant secondary tumor (5). Extravasation is a crucial step of the metastatic process, during which tumor cells roll on the inner vessel lining, establish tight adhesion to endothelial cells, and undergo transendothelial migration (6,7).

To better understand cancer cell interactions with its environment and bypass the species barrier in preclinical models, co-culture and 3D cultures of human cells have been developed (8). One of the main difficulties in developing *in vitro* cancer models is that static 2D cultures predominantly drive high rates of cancer cell proliferation, while tumor cells in various human organs display varying levels of growth and differentiation *in vivo*. The properties of tumor growth and their responses to drugs can vary greatly depending on the specific organ environment. Consequently, most drug development efforts focus on finding therapies that inhibit proliferation, while testing for drugs that target disseminated cells in different stages remains difficult. Although more sophisticated *in vitro* human cancer models have been created to study various tumor behaviors (e.g., growth, migration, invasion, angiogenesis, extravasation, and drug responses) (9–11), few replicate the complex organ-level patterns of cancer growth or therapeutic outcomes seen in patients.

In vivo models such as mice and zebrafish have been instrumental in dissecting this process with spatiotemporal resolution (12,13). Zebrafish embryos, due to their transparency and rapid development, allow real-time imaging of tumor cell arrest, endothelial docking, and transmigration (14,15) , while intravital microscopy in mice enables organ-specific analysis, particularly in brain and lung metastasis models (16,17). Extravasation is modulated by biomechanical constraints such as vessel geometry, flow shear stress, and endothelial contractility (14,18), as well as by pre-metastatic niche priming *via* tumor-derived extracellular vesicles (19). Molecularly, this step involves actin-rich invadopodia driven by Tks5 and Src signaling (20,21), matrix remodeling via MMP2/9/14 (22), integrin-mediated adhesion (23), and organ-specific cues such as VCAM1/VLA-4 interactions or S100A9-RAR-ALDH1A1 signaling in brain metastases (24,25). These findings highlight the coordinated interplay between tumor-intrinsic invasive programs and the dynamic physical and cellular landscape of the metastatic microenvironment.

However, despite their strengths, current in vivo models face key limitations. Zebrafish embryos lack a fully mature immune system and adult tissue architecture, while murine models often rely on immunocompromised backgrounds and simplified tumor cell injections that bypass early dissemination steps. Moreover, the low frequency and stochastic nature of extravasation events, combined with technical challenges in isolating and characterizing rare extravasated cells in situ, limit molecular resolution (26). Finally, interspecies differences in endothelial biology and niche composition constrain the translatability of findings to human disease, underscoring the need for integrated multi-model and microphysiological approaches.

To address these gaps, human-based *in vitro* orthotopic cancer models have been developed using organ-on-a-chip technology. Organ-on-chips are microfluidic cell culture devices incorporating living cells into continuously perfused hollow microchannels, mimicking organ-level (patho)physiology. By recreating the multicellular structures, tissue interfaces, chemical gradients, mechanical forces, and vascular perfusion found in the body, these devices achieve tissue and organ functionality that surpasses what is possible with conventional 2D or 3D culture systems **(27)**. Traditional cell culture models, such as Petri dishes, do not incorporate the cell-cell and cell-matrix interactions and are not suited to address 3-dimensional tissue contexts. A traditional model used to study the invasion or migration of tumor cells *in vitro* is based on the Boyden chamber system **(28)**. Despite its easy use, the Boyden chamber does not allow the application of a flow that seems to play a physiological role in the extravasation process. Recently, 3D cell culture models using microfluidics have been developed and may be used to better mimic and study cell extravasation. New microfluidic-based platforms, including a functional blood vessel model, provide a better solution in allowing direct control of several biochemical and biophysical parameters that are known to influence extravasation as gradients of cytokines **(29,30)**. Microfluidic platforms enable the modeling of specific organ microenvironments and give optical access for continuous monitoring and recording events of interest within the device.

Different chips have been published in the past few years **(30–35)** that mimic a vascular-like structure and allow the study of the extravasation process by following cells, modulating the micro-environment, and changing the flow rate. Some of them could identify new actors in the extravasation process **(34,35)**. *Hajal et al*. showed, in a three-dimensional in vitro blood-brain barrier microvascular model, that astrocytes promote cancer cell transmigration *via* the secretion of C-C motif chemokine ligand 2 (CCL2). This chemokine, then, promotes the chemotaxis and chemokinesis of cancer cells *via* the C-C chemokine receptor type 2 (CCR2), with no notable changes in vascular permeability **(34)**. Using a dual-organ chip, *Liu et al*. demonstrated that the protein expression of Aldo-keto reductase family 1 B10 (AKR1B10) was significantly elevated in lung cancer brain metastasis **(35)**. However, the characterization of metastatic cancer cells according to specific niches still needs to be elucidated.

To address this issue, we developed an original biomimetic microchip with a specific new design, allowing us to study and follow in real-time immune and cancer cells and their interactions with the endothelium wall, and to collect the extravasated cells to characterize them. This device comprises three parts: one microfluidic channel, a collecting chamber, and a porous membrane sandwiched

between them. The upper channel positioned on the membrane is seeded with human umbilical vein endothelial cells (HUVECs) to mimic a complex vascular network. The bottom chamber acts as a reservoir to collect extravasated tumor cells and modulate the metastatic niche's microenvironment.

This new, original microfluidic chip enables the study of real-time immune cell and cancer cell extravasation and their interaction with the endothelium under different conditions. Thanks to the adjustable bottom collecting chamber, the device also allows the collection of these cells for further characterization.

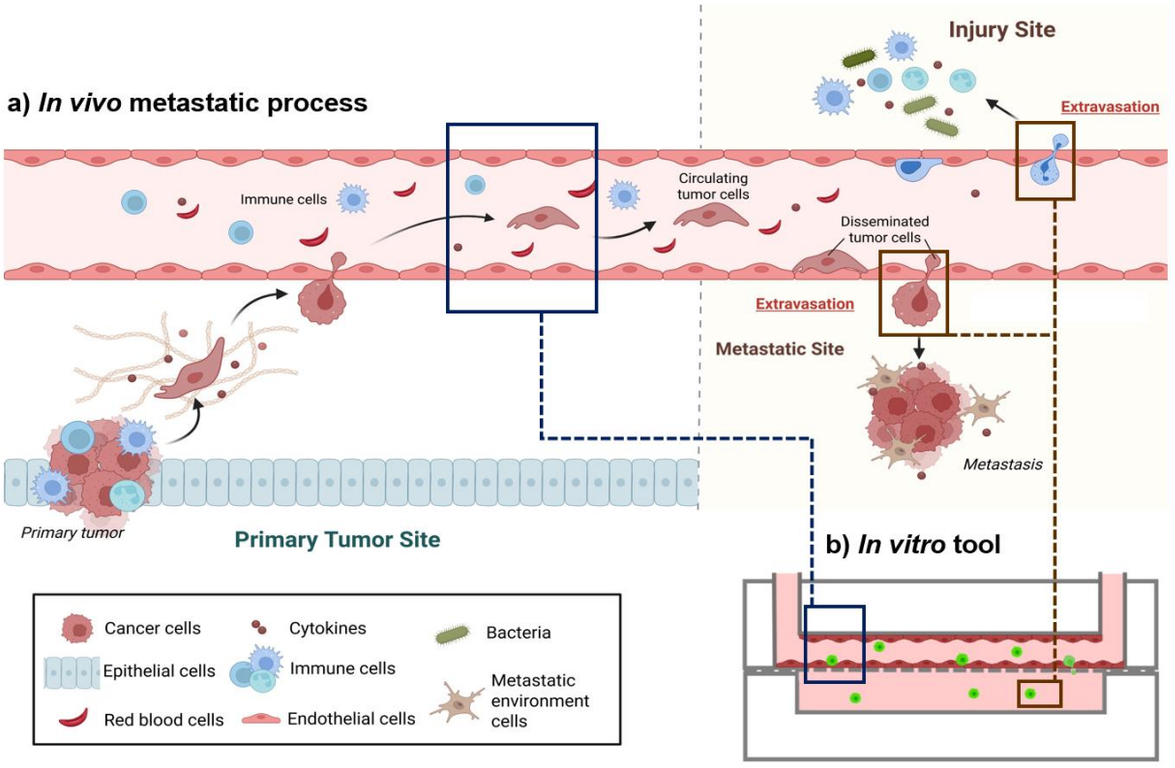

Figure 1. Blood-borne metastatic and immune escape cascade and schematic view of our device. a) Tumor cells escape from the primary tumor site by epithelial-mesenchymal transition, reach blood vessels, and circulate throughout the body. Some of them adhere to the endothelial cells and extravasate in a new environment, forming a micro- and then a macrometastasis. During inflammation, immune cells are recruited to the injury site by via blood vessels and extravasation process. b) The microfluidic tool developed here aims to mimic an endothelial-like structure in the upper channel, where cancer or immune cells can be injected and then collected after extravasation in the bottom channel for characterization.

Material and Methods

Microfabrication.

The microfluidic network was fabricated using a silicon-based master mold. Prime-grade CZ silicon wafers (Siltronix), with a diameter of 76.2 ± 0.3 mm, a thickness of 380 ± 25 µm, a <100> crystal orientation, p-type boron doping, and resistivity ranging from 1 to 10 Ω·cm, were employed as the substrate. Selective etching of the silicon surface was achieved through the application of a negative photoresist mask. A 10 µm thick layer of AZ15nXT photoresist (MicroChemicals) was spin-coated onto the wafer at 1500 rpm with an acceleration of 3000 rpm·s^{-1} for 40 seconds. The coated substrate was soft-baked on a hotplate at 110 °C for 3 minutes. UV exposure was then carried out at a wavelength of 365 nm for 45 seconds at 10 mW. A post-exposure bake was performed for 1 minute at 120 °C. Development was completed using MIF 326 developer (MicroChemicals) for 4 minutes, followed by a 15-second rinse in deionized water.Deep reactive ion etching (DRIE) of the silicon was performed using the Bosch process on an STS DRIE plasma etching system. This alternating process employed C_4F_8 for passivation and SF_6 for etching, with the following parameters: C_4F_8 flow rate of 100 sccm, passivation time of 2.2 s (RIE/ICP power: 20 W / 1500 W), SF_6 flow rate of 450 sccm, and etching time of 3 s (RIE/ICP power: 50 W / 2200 W). During etching, the substrate holder was cooled to –10 °C to enhance thermal dissipation. An etch rate of approximately 5.5 µm/min was achieved, yielding a total etch depth of 150 µm, suitable for the microfluidic channel structures. To facilitate demolding during the PDMS replication step, a thin fluoropolymer (Teflon-like) coating was deposited onto the silicon mold via C_4F_8 plasma treatment.

The microfluidic device is composed of two polydimethylsiloxane (PDMS) layers. PDMS pieces are synthesized following the manufacturer's protocol. Briefly, a PDMS mixture (Sylgard 184 Silicone Elastomer Kit, Dow chemicals, Ellsworth Adhesives France, Pontoise, France) with a monomer: curing agent ratio of 10:1. The mixture is placed in a desiccator for two hours to remove trapped air bubbles. Then, PDMS is poured on the silicon mold. The PDMS layer is cured in an oven at 70°C for 4 hours. PDMS is then released from its mold. The upper PDMS layer's rectangular shape (50 mm x 20 mm) is cut, and fluidic inlets and outlets are punched with a 1.2 mm Ø biopunch. A thin PDMS layer (1 mm thickness) intended for the collecting chamber is produced using the same process as for the top layer. This layer is then cut into a rectangular shape of the same dimensions as the PDMS top layer. The inner part of this layer is cut to create a hole just below the upper channels. A plasma treatment (Corona SB, BlackHole Lab, France) is then applied on this thin PDMS layer as well as on a rectangular glass slide (75 mm x 25 mm), followed by assembly and heat activation at 70°C for 1 hour to make irreversible bonding between PDMS and glass. In the first step of the experimentation, a polycarbonate membrane (it4ip, PC ipCellCulture, 8 µm pores, 20 µm thickness) is deposited on a rectangular glass slide. The whole PDMS top layer, polycarbonate membrane, and glass slide are assembled using a specific holder to prevent leakage during perfusion of the upper channels. At day 3, when a complete 3D endothelial layer is obtained throughout the entire device, the holder is opened, and the rectangular glass slide is replaced by the PDMS collecting chamber filled with culture medium. The holder is closed again to carry on the experiment. The chips are stored in a sterile petri dish at room temperature until use. The device is connected to a microfluidic flow control system using a mid-pressure syringe pump (Mid Pressure Module, Nemesys, Cetoni) equipped with Hamilton glass syringes to limit gas exchange during the experiment.

Cell culture.

Primary human umbilical vein endothelial cells (HUVECs pooled, Lonza C2519A) are cultured in complete culture medium (Gibco Medium 200) supplemented with 2% low serum growth supplement kit (LSGS kit, Gibco) and 0.4 % Penicillin-streptomycin 10 000 U/ml (Gibco). All experiments are carried out using HUVECs between passages 4 and 5. MDA-MB-231 cells from ATCC are cultured in DMEM (Eurobio) supplemented with 10% FBS (Gibco, Qualified, US origin, standard sterile filtered) and 0.4 % penicillin-streptomycin. The MDA-MB-231 cell line, derived from human breast adenocarcinoma, is a highly aggressive, invasive, and poorly differentiated triple-negative breast cancer (TNBC) cell line. GFP-transfected MDA-MB-231 cells are previously established in (36) and named as MDA-MB-231 GFP thereafter. They are cultured in the same medium as MDA-MB-231 WT. Normal Human Lung Fibroblasts (NHLF, Lonza CC-2512) are cultured in basal culture medium (Lonza, FBM basal medium, cc-3131) supplemented with FGM-2 SingleQuots (Lonza, cc-4126) and 0.4 % penicillin-streptomycin. Cells are detached from the culture flask using TripLe Express Enzyme 1X (Gibco). PBS 1X (Gibco, pH 7.4 without calcium and magnesium) is used for rinsing after coating steps. TNF-α at a concentration of 10 ng/ml in complete medium 200 (R&D Systems, recombinant Human TNF-α Protein, 210-TA-005) is used for endothelium inflammation. CXCL12 (RD Systems, 350-NS-010) is used as a chemokine attractant at a 100 ng/ml concentration in a complete medium 200.

Channel coating and HUVECs seeding in the microfluidic channel.

To generate 3D functional biomimetic blood vessels, the inner surfaces are coated with collagen type I (from rat tail, Corning, 354249, at a concentration of 100 µg/ml) and fibronectin (from human plasma, Sigma, F0895, at a concentration of 50 µg/ml). The collagen solution is injected into the device and left for 1 hour at 37°C. After a washing step at 100 µl/min with PBS 1X for 10 min, the fibronectin solution is injected into the device and left overnight at 37°C. A washing step with a complete culture medium is applied the following day. A suspension of 5.10^7 HUVECs/ml is injected into the upper channel. HUVECs can settle for 4 hours under static conditions in a CO_2 incubator. HUVECs are then cultured under dynamic conditions for 3 days with a stepwise flow increase, starting at 6 µl/min on the first day and increasing to 24 µl/min on day 3.

HL60 and MDA-MB-231 GFP injection.

At day 3, once a complete 3D endothelium is obtained, the medium contained in the syringe is replaced by medium enriched with or without 10 ng/ml of TNF-α. This TNF-α enriched medium is perfused on the HUVECs layer for 24 hours before the HL60 or MDA-MB-231 GFP injection. On day 4, the whole PDMS top layer and the porous PC membrane are placed above the collecting chamber filled with complete culture medium enriched with or without 100 ng/ml of CXCL12. A total of 10^6 MDA-MB-231 GFP cells are injected through the septum of the microfluidic tubing using 21G needle, using a solution at a concentration of $2x10^6$ cells/mL. During cell injection, the flow rate is maintained at 10 µL/min (1 dynes/cm^2) and then progressively increased to 24 µL/min (2.4 dynes/cm^2) for 24h.

Immunofluorescence staining.

On day 5, 24 hours after MDA-MB-231 GFP cells injection, the cells inside the device (HUVECs and MDA-MB-231 cells) are fixed using 50 µl of paraformaldehyde (PFA) 4% in PBS 1X. After washing using PBS 1X, a saturation step is performed using FBS 5% in PBS 1X for 1 hour at room temperature. Then, a primary antibody against CD31 (Invitrogen, MA513188) is injected at a dilution of 1/10 for 1 hour at room temperature. A primary antibody against VE-cadherin (Santa-Cruz, SC- 9989) at a dilution of 1/200 is also used to verify the presence of adherent junctions. A secondary antibody Alexa Fluor 546 (A11030, Invitrogen) is injected at a dilution of 1/500 for 1 hour at room temperature. Finally, the nuclei are marked with Hoechst 33258 (Sigma, Bisbenzimide H 33258) at 200 µM for 30 min. The device is kept in the dark at 4°C before fluorescence imaging.

Microscopy.

Time-lapse experiments during and after MDA-MB-231 GFP injection are performed in a CO_2- and temperature-controlled Leica DMi8 microscope. Bright-field images for HUVECs and GFP fluorescence images for MDA-MB-231 cells are monitored to follow the dynamic extravasation process. Different regions of interest (ROIs) are chosen along the channel network to record arrest events of MDA-MB-231 cells on the endothelium layer or the extravasation process across the endothelium wall. After fixation and immunofluorescence staining, the device is imaged on an SP8 confocal microscope using a water-immersive 25 X objective with a step size ranging from 10 to 15 µm.

Genes expression analysis.

Cells are lysed in TRIzol (Thermofisher Scientific, Illkirch, France), cell extracts are recovered, and total RNAs are purified by phenol/chloroform extraction and precipitation. RNAs are quantified on a NanodropOne (Thermofisher Scientific), and reverse transcription reactions are carried out using a high-capacity cDNA reverse transcription kit with an RNase inhibitor (Applied Biosystems, Thermofisher Scientific). Quantitative duplex PCR is performed using cDNA mixed with a TaqMan FAM-labeled probe for the target gene (Thermo Fisher Scientific) and a β2-microglobulin VIC-labeled probe.The list of primers can be find in *Delannoy et al.*(37) Reactions are run on a StepOne machine. We also use Taqman Array custom Cards (ThermoFisher Scientific), 100 ng of RT products are loaded in the Cards, and amplifications are performed using a QuantStudio7 Flex machine. C_q values are calculated at the upper linear range of the logarithm-2 amplification curve using the StepOne v2.3 software. Data are expressed as $2^{-\Delta\Delta Cq}$ where ΔCq = Cq of the transcript of interest - Cq of reference (B2M) measured in the same tube, and ΔΔCq = mean ΔCq experimental samples - mean ΔCq control samples of the same experiment. Relative quantity (RQ) is $2^{-\Delta\Delta Cq}$ (38). NHLF were used as negative controls within the HUVEC characterization study as described in (39) and (40), to validate the specifics of gene expression in HUVEC with or without stimulation/flow.

Statistics.

All experiments were performed at least twice in similar conditions; n indicates the numbers of biological replicates per shown experiment. Statistical analyses were performed using the multiple t test or the student's t-test using the GraphPad Prism 8.

Graphs, drawings, and image generations.

Illustrations are created on *Biorender*. Graphs are generated on the *GraphPad Prism 8* software. Microscopy images are analyzed and processed on the *Fiji* and Imaris software. The alignment of actin filaments is quantified using the Fiji software's plug-in " Directionality," and the analysis is performed on 1500 events.

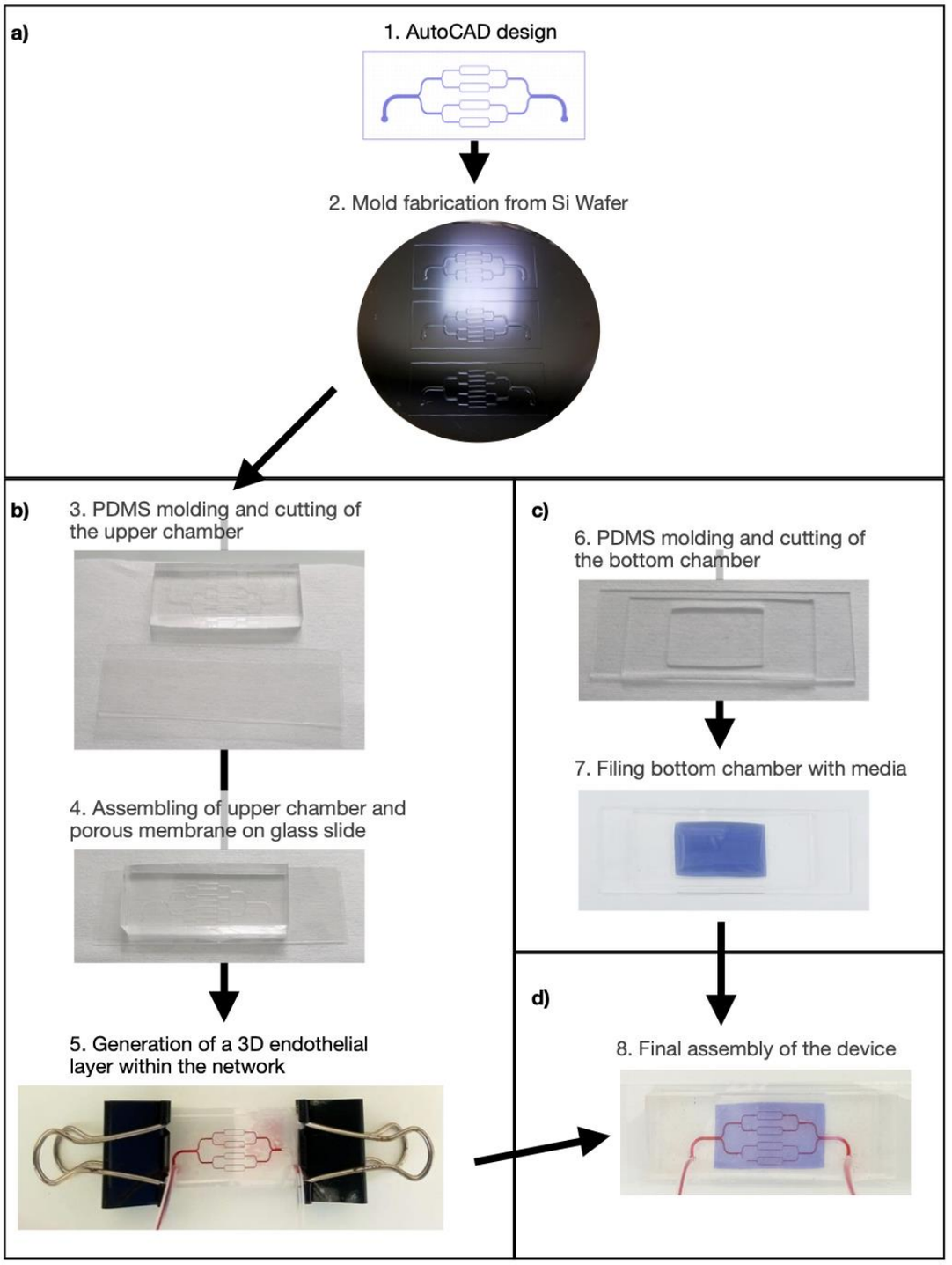

Figure 2. Step-by-step microfluidic device fabrication process (See Material and Methods for details). **a)** Design and fabrication of the wafer mold for the upper chamber. **b)** Assembly of the upper chamber with the porous membrane onto a glass slide, tubing connection, and formation of the 3D endothelial layer. **c)** Fabrication of the bottom "collecting" chamber and preparation for final assembly by filling it with culture medium. **d)** Final assembly of the upper vascular network with the bottom chamber for the extravasation experiment.

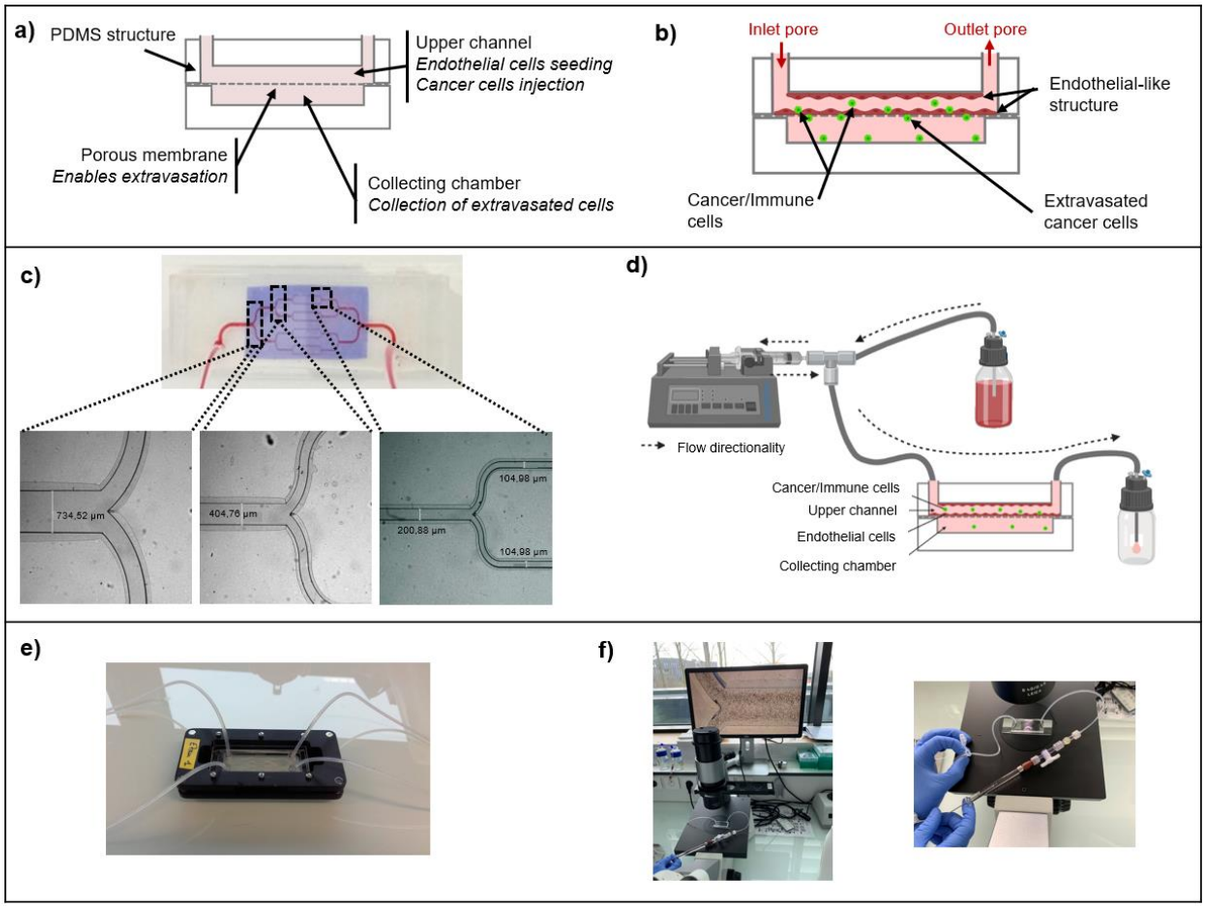

Figure. 3 Microfluidic design. **a)** Representation of the microfluidic device. **b)** Representation of the microfluidic device after endothelial-like structure obtention and cancer/immune cells injection. **c)** Complete device assembled. The upper part of the device mimics the vascular network filled with red ink, and the lower collecting chamber is filled with blue ink. Magnified views of the four channel types, ranging from 800 µm to 100 µm in width. **d)** Scheme of the complete setup with flow directionality. **e)** Picture of the complete device assembled. **f)** Pictures of the chip during HUVEC injection.

Results

Development of the microfluidic device.

We created a biomimetic microchip designed to study immune and cancer cells' interactions with the endothelium wall in real-time and collect extravasated cells for analysis. The device has three parts: a microfluidic channel, a collecting chamber, and a porous membrane between them **(Figure 1)**. The upper chamber mimics microvasculature, while the lower chamber simulates a metastatic niche with a tailored chemoattractive microenvironment **(Figure 3).**

We designed our device to be a two "chambers" device separated by a porous membrane, allowing cells with migratory potential to go from one to the other. We used a 20 µm-thick membrane with 8 µm pores to model the endothelial barrier and study metastatic extravasation. The 8 µm pore size permits the transmigration of single cancer cells while mimicking physiological endothelial gaps (41,42). The 20 µm thickness ensures mechanical stability during microfluidic assembly and flow application, while remaining compatible with high-resolution imaging. This configuration also supports HUVEC monolayer formation and barrier function (43), and is consistent with transwell and organ-on-chip models used to study tumor cell extravasation (30,44). Also, we chose to design the upper "chamber", the microfluidic network, to mimic a microvascular network resembling natural blood vessels, with an 800 µm wide entrance channel that splits into two half-width channels, further dividing into up to eight 100 µm channels at the device center before symmetrically merging. The device maintains a uniform height of 100 µm along the network. At the opposite, the bottom chamber of the device is one single chamber covering the full area of the network. The later will be used to collect transmigrating cells from the flow running with the endothelial structure to the static environment.

Design and mold. We used the Fusion 360 software (Autodesk Fusion 360 2020, v2.0.10440) to design the network of the upper chamber (Figure 2) (See *Material and Methods* for more details). Photoresist is spun on the Silicon wafer, and the Fusion design used as a mask for Deep Reactive Ion Etching (DRIE), where 100-µm-deep structures (channels) are defined. For practicability to other within the community, we also generate from Computer-Aided Design (CAD) files using Autodesk Fusion 360 (version 2.0.10440, 2020) to be imported into a Datron NEO CNC machining center (Datron, Sevrier, France) to mille an aluminum mold (cf Supplemental data, Fig Suppl 7 and 8).

PDMS upper network layer. A PDMS mixture, incubated in a desiccator for two hours to remove trapped air bubbles, is poured on the mold. The PDMS layer is cured in an oven at 70°C for 4 hours. PDMS is then released from its mold. The upper PDMS layer's rectangular shape (50 mm x 20 mm) is cut, and fluidic inlets and outlets are punched with a 1.2 mm Ø biopunch to plug tubing to allow fluid perfusion via syringe pumps.

Porous membrane and Microfluidic. In the first step of the experimentation (to generate the endothelial capillary network, a polycarbonate membrane (it4ip, PC ipCellCulture, 8 µm pores, 20 µm thickness) is deposited on a rectangular glass slide. The whole PDMS top layer, polycarbonate membrane, and glass slide are assembled using a specific holder to prevent leakage during perfusion of the upper channels. The device is connected to a microfluidic flow control system using a mid-pressure syringe pump (Mid Pressure Module, Nemesys, Cetoni) equipped with Hamilton glass syringes to limit gas exchange during the experiment, filed with pre-equilibrated media in temperature (37°C) and CO_2 controlled incubator.

PDMS collecting layer. For the collecting lower chamber, a thin PDMS layer (1 mm thickness) intended for the collecting chamber is produced using the same process as for the top layer within a blank mold, with a rectangular shape of the same dimensions as the PDMS top layer. The inner part of this layer is cut to create a hole just below the upper channels. A plasma treatment (Corona SB, BlackHole Lab, France) is then applied on this thin PDMS layer as well as on a rectangular glass slide

(75 mm x 25 mm), followed by assembly and heat activation at 70°C for 1 hour to make irreversible bonding between PDMS and glass.

Full device assembly. After the 3 days of building up the endothelial 3D layer (cf paragraph "***Obtention of an endothelial-like structure***"), the PDMS upper and lower parts (after been field with media) are carefully aligned to ensure that all the bifurcation networks of the upper channel are positioned over the hole. The holder is closed again to carry on the experiment by injecting cancer cells or immune cells.

The bottom layer acts as a reservoir to collect tumor cells that extravasate. This collecting chamber serves as a dynamic metastatic niche, allowing for controlled modifications with specific factors or stroma to establish a chemoattractive microenvironment. In our experiment, CXCL12 is introduced to create a localized chemokine gradient that stimulates tumor cell extravasation (cf paragraph "***Microfluidic platform for monitoring*** cell ***interaction with the endothelium***" and "***A platform to collect extravasating cancer cells***").

Obtention of an endothelial 3D-like structure.

Physiological shear stress in veins and large arteries ranges between 1-10 dynes/cm^2 and 10-60 dynes/cm^2, respectively (45,46). In the microfluidic channels, the fluid flow generates the shear stress. This concept is based on the laminar flow Navier-Stokes theory since the flow in the microfluidic channel is laminar, Newtonian, and incompressible. For a rectangular channel of dimensions w x h x L with h < w « L, the wall shear stress can be approximated by the following equation 1 (47,48):

$$\boldsymbol{\tau} = \frac{\boldsymbol{6.\mu.Q}}{\boldsymbol{w.h^2}}. \quad (1)$$

Where τ is the wall shear stress in dynes/cm^2, μ is the viscosity of medium (μ=0.0078s.dynes/cm^2 for standard culture medium), Q is the flow rate (m^3/s), w the width (m), h the height (m), and L is the length of the channel (m). As the height of the branched channel network of the device is kept constant (≈ 100 μm) throughout the network, and the width is divided into two branches at each bifurcation, the flow rate is divided into two at each bifurcation, and so the wall shear stress is maintained constant throughout the network. The upper part of the device is perfused with a complete culture medium under different flow rates using syringe pumps. Before cell seeding, the upper channel's inner surface is coated with fibronectin and collagen. These inner surface coatings of both PDMS and PC membranes are essential to induce HUVECs adhesion on both surfaces.

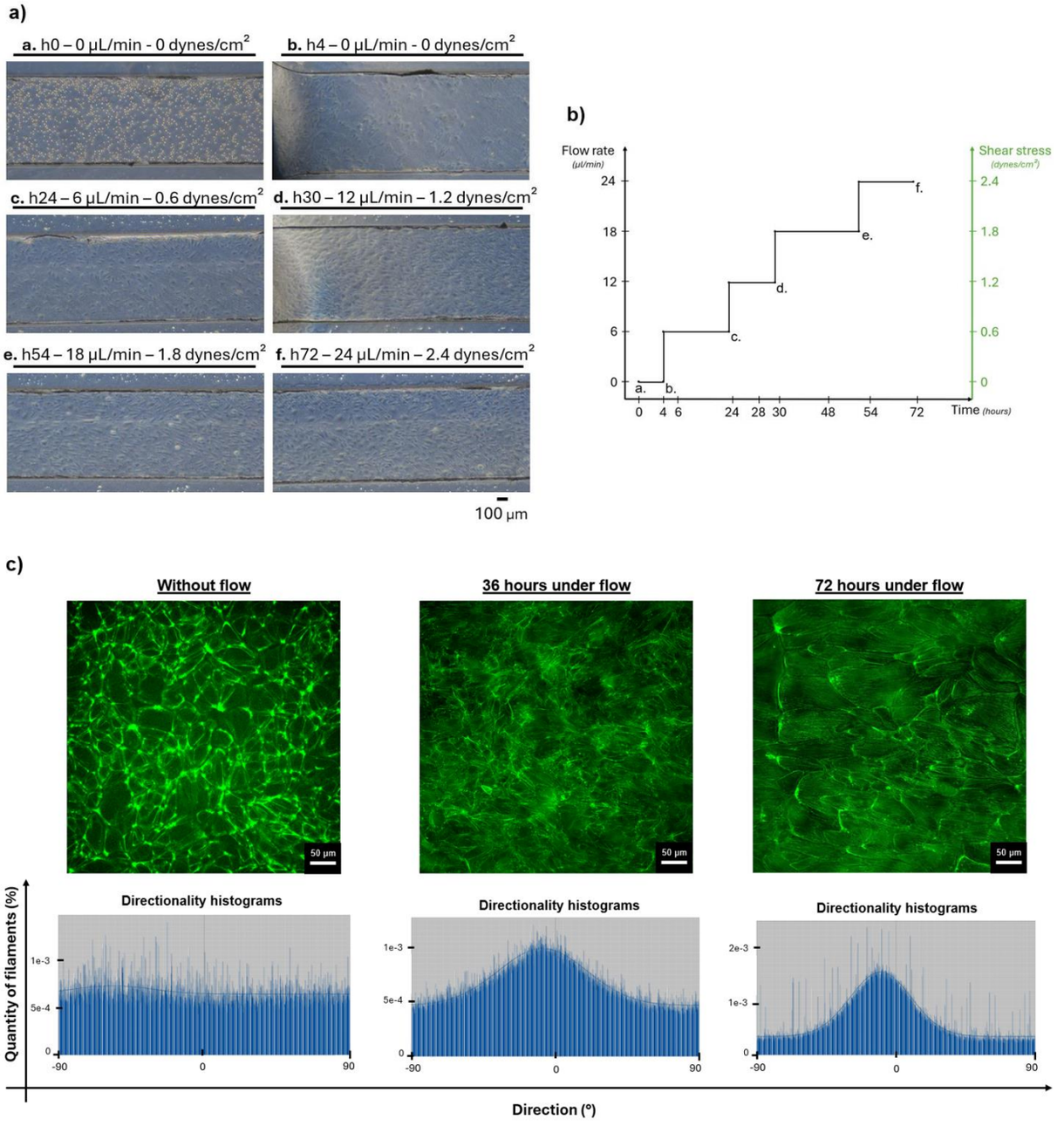

Figure. 4 Impact of dynamic culture on HUVECs. a) Brightfield images of HUVECs culture under a progressive flow in an 800 µm large channel (5X). **b)** Progressive increase of the flow rate and corresponding shear stress over time to obtain a complete and 3D endothelial-like structure. **c)** Impact of the flow on actin filament alignment in HUVEC – in static conditions ; during 36 hours under progressive flow ; or during 72 hours under progressive flow (green : phalloidin labeling conjugated with alexa fluor 488, showing actin filaments).

Following cell seeding, HUVECs initially adhered to the PC membrane at the bottom of the channel. By day 2 of flow culture, their proliferation led to complete coverage of the PDMS roof. HUVECs proliferation then slowed, and a complete 3D endothelium is formed between day 2 and day 3. Additionally, to mimic the physiological shear stress and promote the formation of a 3D structure, a complete culture medium is perfused 4 hours after HUVECs seeding, at

a flow rate of 6 µl/min, creating a shear stress of 0.6 dynes/cm^2. The flow level is then increased step-by-step for 3 days to reach 24 µl/min (2.4 dynes/cm^2) (**Figure 4a-b** in channel 800 µm; see ***Figure supp 1*** for the other sizes). Linear flow increases and flow stability has been validated (Figure supp 9 and 10). This gradual increase in flow rate is required to induce HUVEC proliferation during the initial stage, followed by elongation in the flow direction. In fact, the culture of HUVECs under flow conditions promotes an alignment of actin fibers. Compared to cells cultured in static conditions, HUVECs exposed to fluidic conditions exhibit a uniform alignment of actin filaments in the direction of the flow (**Figure 4c**).

Anti-CD31 immunofluorescence staining combined with confocal microscopy observations reveals a tight and confluent endothelial monolayer spanning the channels' inner surface 4 days after HUVECs seeding (**Figure 5a.**). Interestingly, we also observed really few gaps through the endothelial layer. In parallel, VE-cadherin immunofluorescence staining was performed on day 4 of dynamic culture conditions and revealed the presence of adherent junctions on all the channel surfaces of the device (**Figure 5b**.). Confocal images obtained in smaller capillary size, orthogonal projection, and a 3D animation movie of the channel can be found as supplementary materials (***Figure supp 2-3*** & ***Movie 1S-3S***). Confocal images reveal that 3D biomimetic blood vessels were successfully generated in a reproducible manner.

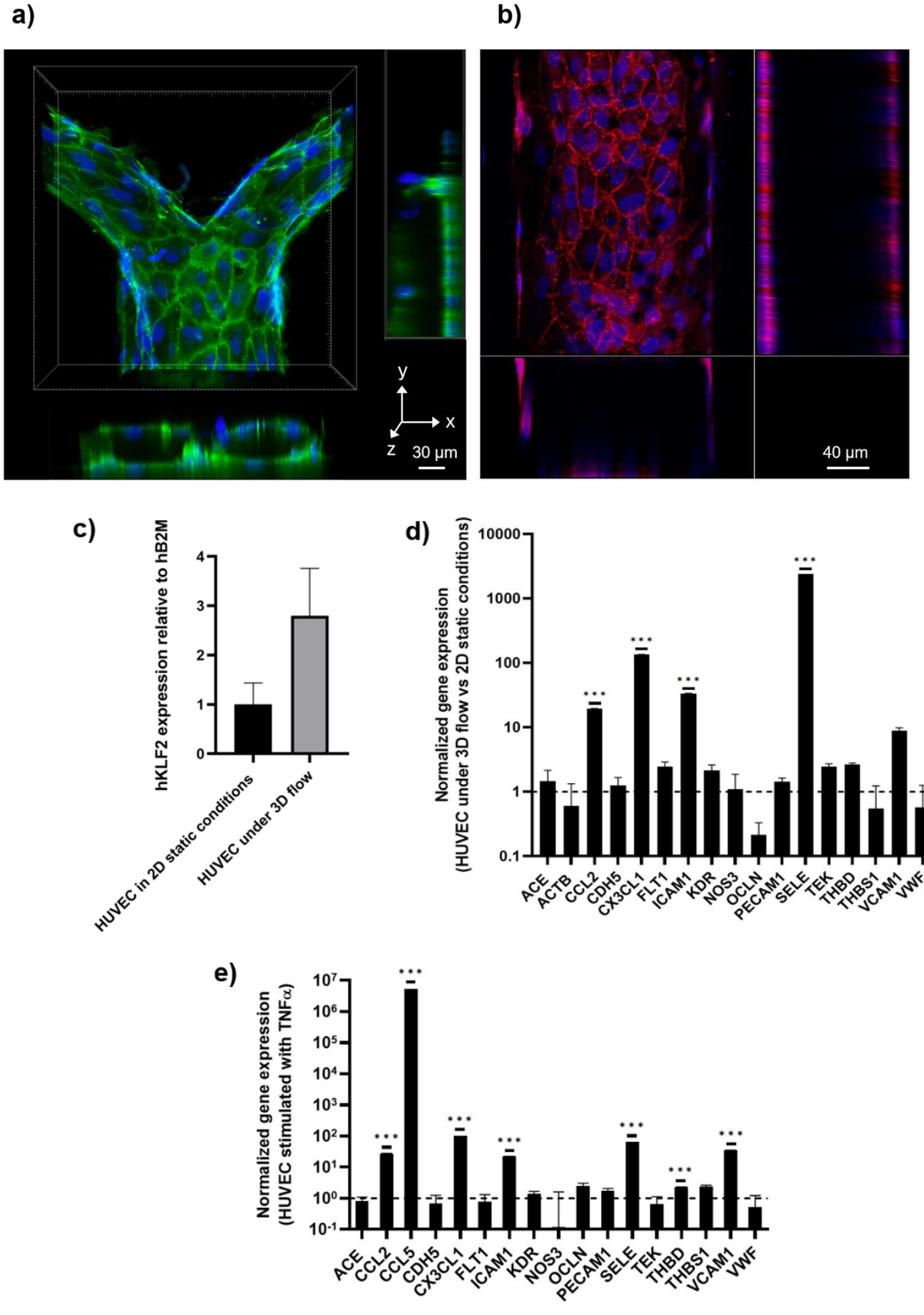

Figure 5. Characterization of the endothelial-like structure. a) Confocal images. Anti-CD31 staining (green) and Hoechst (blue) immunofluorescencestaining of HUVECs inside the device at day 4 of the dynamic culture condition. Orthogonal views inside a 400 to 200 µm channel width. **b) Confocal images.** VE-cadherin (red) and Hoechst (blue) immunofluorescence staining of HUVECs inside the device at day 4 of dynamic culture condition, inside a 200 *µm* channel width. **c)** Expression levels of KLF2 between HUVECs grown in microfluidic devices in 2D static and in 3D flow conditions (*n=3* ; *t test, p-value = 0,189*). **d)** Comparison of the expression levels of genes between HUVECs grown in 2D static and 3D flow conditions (*n=3* ; *Multiple t test*, *q-value *** < 0,0001*). **e)** Expression levels of genes in HUVECs in microdevices and stimulated or not with 10 ng/ml of TNFα for 16 hours (*n=3)* ; *Multiple t test, q-value *** < 0,0001*).

Characterization of the endothelial-like structure

Genetic analyses were performed to further examine HUVECs lining the channel surface of the devices. First, gene expression levels in HUVECs and NHLF grown in 2D under static conditions were analyzed to confirm the endothelial phenotype of the primary cells used. Compared to NHLF, HUVECs exhibited much higher levels of VE-cadherin (CDH5), VEGF receptors FLT1 and KDR, endothelial-specific NO synthase NOS3, angiopoietin receptor Tie2 (TEK), leukocyte adhesion receptors ICAM1, VCAM1, and SELE, PECAM1, and vWF, among selected marker genes (***Figure supp 4***), thus validating the endothelial phenotype of the primary HUVECs. Next, we evaluated whether the establishment of these HUVECs in the microdevices in flow for 4 days had any impact on the cell gene expression profile. Of note, flow conditions induced a marked increase in expression levels of the KLF2 gene, a key transcription factor known to be upregulated by flow in perfused HUVECs (49,50) (**Figure 5c**). While HUVECs grown in microdevices displayed a mostly similar gene expression signature to HUVECs grown in static, 2D conditions on plastic, we could observe an upregulation of CCL2, CX3CL1, ICAM-1, SELE & VCAM-1 gene expression (**Figure 5d**).

To assess whether the endothelial cells placed in the microfluidic devices were responsive to inflammatory cytokines, microvessels were stimulated or not with 10 ng/ml TNFα for 16 hours, and gene expression was assessed via RT-qPCR. HUVECs in microdevices showed a significant increase in expression of CCL2, RANTES (CCL5), CX3CL1, ICAM-1, SELE, and VCAM-1 and a down-regulation of NOS3, in strong correlation with previous reports using HUVECS in 2D static conditions (**Figure 5e**).

Altogether, these observations confirm that HUVECs placed in the microfluidic devices retain their endothelial phenotype, remain responsive to pro-inflammatory signals when stimulated, and activate the expected repertoire of genes under these conditions (51–53).

Microfluidic platform for monitoring leukocyte (HL60) and metastatic breast cancer cell (MDA-MB-231) interaction with the endothelium

As proof of concept, we first used HL-60 cells, a promyeloblast cell line, expressing GFP. On day 3, after forming a 3D endothelial network, endothelial cells were activated with TNF-α for 24 hours. Subsequently, 10^6 GFP-HL-60 cells were introduced into the chip flow, and images were captured in specific areas of the device using a Nikon T2 fluorescent microscope in controlled environmental conditions (37°C, 20% O_2, 5% CO_2).

We observed that most HL-60 cells did not adhere to the activated endothelium. However, as expected, a small subset of cells adhered and migrated along the endothelial surface against the flow. These cells subsequently transmigrated by disrupting the integrity of endothelial tight junctions, creating entry points by physically displacing endothelial cells. This allowed HL-60 cells to penetrate the endothelial layer and invade the subendothelial space. Once beneath the endothelium, the transmigrated HL-60 cells continued to migrate, displaying movement characteristics of amoeboid migration. This type of migration relies on dynamic cytoplasmic projections, or blebs, which enable the cells to navigate through narrow spaces without degrading the surrounding extracellular matrix (***Movie 4S to 7S***).

On the other hand, we used the metastatic cancer cell line MDA-MB-231 to study their adhesion to and transmigration through the endothelial layer. On day 3, after the formation of a complete 3D endothelium throughout the network, the chip holder was opened, and the glass slide was replaced by the bottom collecting chamber filled with the medium. To follow the early events of cancer cell transmigration, the microdevice was maintained in a humidified environment, and a Temperature/CO_2 control box was placed on a microscope stage. This enabled real-time follow-up of cancer cells and their interactions with the endothelium. Specifically, GFP-expressing MDA-MB-231 cells, created in-house, were used to study of interactions between this TNBC cell line and the endothelium. A million of MDA-MB-231 GFP cells were injected into the upper channel under perfusion. Arrest and/or extravasation processes were live-recorded for 24 hours after cancer cell injection.

Different ROIs were chosen to live record the MDA-MB-231 cell arrest and/or extravasation process. As others have observed, cell transmigration, if present, should occur quite rapidly after tumor cells arrest on the capillary bed (44). A transmigration speed of 15 µm/h for the MDA-MB-231 cells has been measured experimentally (54), meaning that transendothelial migration across the endothelium and porous membrane should occur within the first hours of our experiments.

The microfluidic device was maintained inside a temperature-, CO_2- and humidity-controlled box and placed on a microscope stage to monitor HUVECs under transmitted light and MDA-MB-231 GFP cells under fluorescent light. One hour after being injected, MDA-MB-231 cells were imaged using GFP expression, while HUVECs were visualized and recorded under brightfield. **Figure 6a** presents the timeline of MDA-MB-231 cells one hour after injection. The motion direction of cancer cells does not seem to follow the flow direction as individual cells move in varying directions. One of the 2 initial cells, adhering to the endothelium, underwent division 3h after injection. Also, one of the daughter cells moved toward the flow while the other daughter cell moved against it. The three cells then clearly crawl and stretch on the endothelium, whether in the direction of the flow or against it. At the end of the video, the motion of the MDA-MB-231 cell seemed to slow down. The cells in the middle seemed to become stuck and began to spread over the endothelium. Throughout the recording, the endothelial wall was continuously reshaped. Endothelial cells aligned and elongated in the direction of the flow. As observed within the Timelapse, the endothelium layer remains intact, without changes within its structure or sign of cell death. We could even see HUVEC decided

few hours (7h) after MDA-MB-231 have been injected. The full video can be found as supplementary material (***Movie 8S to 12S***).

It is worth noting that HL60 and MDA-MB-231 cells adhere randomly to different surfaces of the endothelial layer, not just the bottom one. Moreover, while cells can extravasate through any part of the device, they can only migrate further away from the endothelium by moving downward through the porous membrane, as the other walls are made entirely of PDMS. Also, HL60 and MDA-MB-231 cells do not pass through the few gaps observed on the endothelial layer, but open tight junction between endothelial cells.

Since most MDA-MB-231 cells did not arrest on the endothelium, we aimed to investigate the effect of the HUVECs monolayer activation by TNF-α on the firm adhesion of cancer cells to the endothelium. The HUVECs monolayer was first activated with 10 ng/ml TNF-α for 24 hours. Then, MDA-MB-231 cells were injected inside the top channel underflow. Confocal microscopy revealed that a subpopulation of cells remained attached to the activated endothelial monolayer and could proliferate. When MDA-MB-231 cells did arrest on the endothelium, they often invaded the endothelium and replaced HUVECs, thus damaging the endothelium integrity (***Figure 6b***). A small fraction of MDA-MB-231 cells, approximately a hundred out of a million cells, were arrested on HUVECs monolayer when activated with TNF-α. On the contrary, almost none of the MDA-MB-231 cells remained (less than a dozen or so cells) attached to the non-activated endothelium. We confirmed that the TNF-α inflammation promotes the arrest of MDA-MB-231 cells on the HUVECs wall.

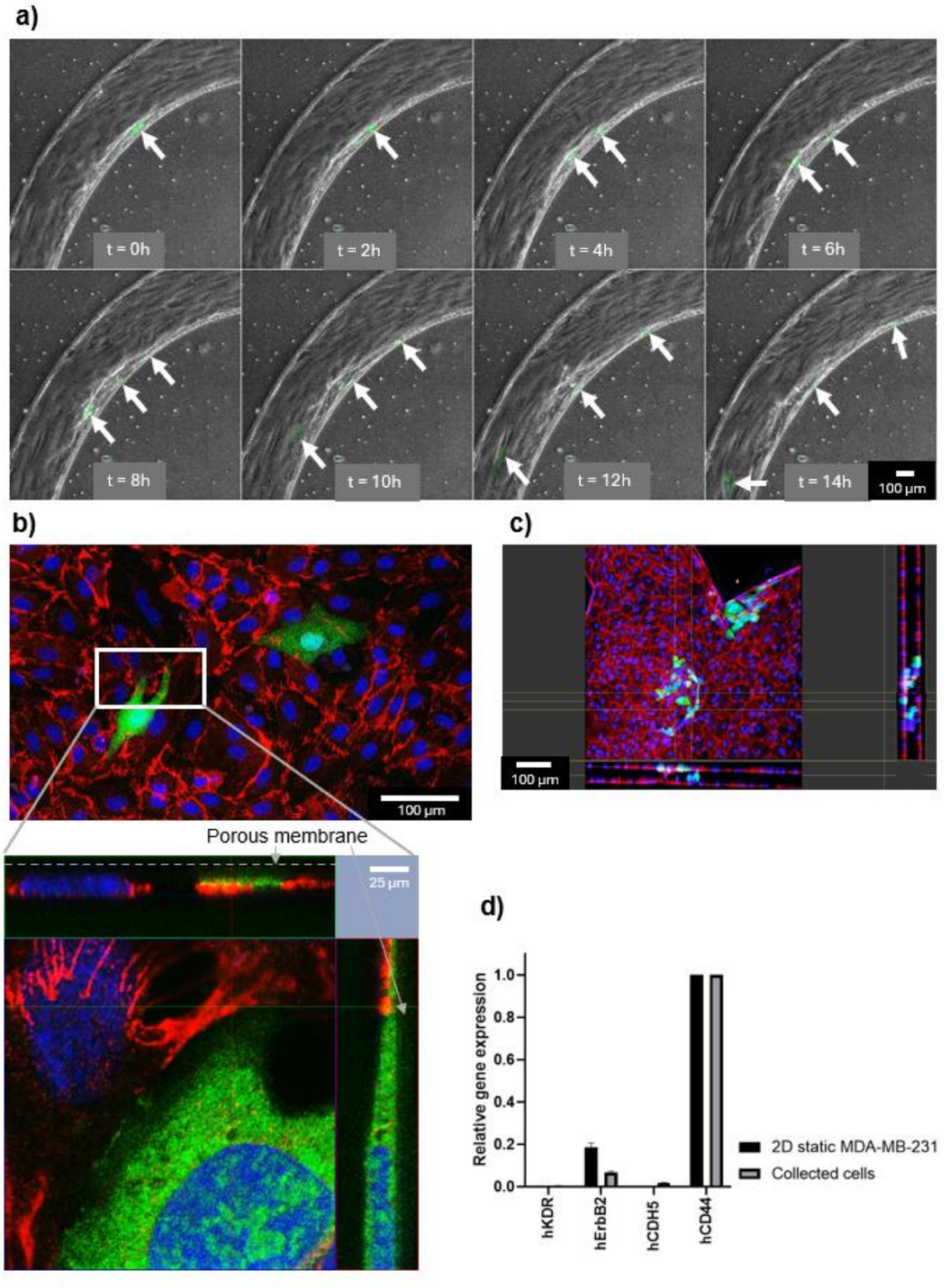

Figure 6. **Following extravasation and collecting extravasated cells. a)** Timeline of interaction between MDA-MB-231-GFP cells (green) and HUVECs endothelium for 14 hours in 200µm channel. Representative images extracted from movie10S. (White small dots are the pores from the porous membrane). **b)** Arrest and beginning of extravasation process of a MDA-MB-231-GFP cells across endothelial cells. CD31 (red) and Hoechst (blue) immunofluorescence staining of HUVECs, and GFP (green) fluorescence for cancer cells. **c)** MDA-MB-231-GFP cells (green) arrested on TNFα activated HUVECs endothelium. **d)** RT-qPCR expression of KDR, ErbB2, VE-Cadherin, CD44 in 2D static MDA-MB-231 cells and in cells collected in the lower chamber of the device after MDA-MB-231 perfusion (*n=2*).

A platform to collect extravasating cancer cells

The bottom collecting chamber acts as a reservoir to collect extravasated tumor cells and allows for the introduction of chemoattractive media. In this study, we wanted to investigate the modulation of the medium inside the bottom chamber. The bottom layer was filled with a complete culture medium with or without CXCL12 (Stromal cell-Derived Factor 1-alpha SDF-1α) at a 100 ng/ml concentration. Some MDA-MB-231 cells could extravasate through the openings of the porous membrane (***Figure 6c,*** ***Figure supp 5***). Once extravasated, MDA-MB-231 cells proliferated underneath the membrane. Animation movies showing extravasated cancer cells can be found as supplementary material.

We used a stitched-confocal microscopy images of the full collecting chamber to count the number of cells passing through the membrane. Our results show that a rare fraction of MDA-MB-231 cells, approximately tens out of a million cells (***Figure Supp 11***), could extravasate when the collecting chamber was supplemented with CXCL12, compared to almost none when the collecting chamber did not contain chemokine. These results indicate that in our conditions, CXCL12 was a prerequisite for the MDA-MB-231 cells to extravasate in the collecting chamber.

As a proof of concept, a gene expression analysis was performed on a dozen or so extravasated cells, which migrated to the bottom of the collecting chamber, to determine whether they were cancer cells, as expected, or endothelial cells that had detached and potentially migrated through the supporting membrane. Twenty four hours after cell injection, we validated the presence of GFP-positive cells at the bottom of the collecting chamber, The device was then opened and cells within the collecting chamber were retrieved using trypsin. These extravasated cells expressed high levels of CD44 and Erb2 and low levels of KDR and CDH5, matching the profile of MDA-MB-231 cells and not of HUVECs, confirming that circulating cancer cells had crossed the microdevice endothelium (***Figure 6d and*** ***Figure supp 7***).

Discussion

This study leveraged an innovative biomimetic 3D microfluidic device designed to investigate and monitor real-time cancer cell interactions with an endothelium. After three days of culture under perfusion, a fully formed 3D endothelial monolayer was successfully established. Immunostaining with anti-CD31 and VE-cadherin confirmed the formation of a confluent 3D monolayer across the entire device. RT-qPCR analyses further validated the endothelial gene expression profile of in-chip HUVECs as well as their pro-inflammatory response to TNF-α induction. Indeed, some pro-inflammatory genes, such as CCL2, CX3CL1, ICAM-1, SELE & VCAM-1, were upregulated, suggesting that an inflammatory activation of the cells occurred in microdevices in these conditions (55). Once the 3D endothelium is fully

established, the chip is placed on a microscope stage within a controlled environment (temperature, CO_2, and humidity). Cancer cells are then injected into the device, and the microfluidic platform, compatible with high-resolution microscopy, enables the tracking of their arrest and subsequent extravasation through transmitted light and fluorescent imaging.

Our findings indicate that TNF-α stimulation is essential to the firm adhesion of MDA-MB-231 cells to the endothelial layer. Following adhesion, these cancer cells disrupt the endothelial integrity by displacing HUVECs. Furthermore, the CXCL12 chemokine was shown to be critical for inducing MDA-MB-231 extravasation through the endothelial layer and across the polycarbonate membrane pores.

Our microfluidic device also facilitates the collection of extravasated cells for downstream analyses, as the collected cancer cells displayed a gene expression signature of MDA-MB-231 cells.

The development of this biomimetic microfluidic device addresses significant gaps in existing models of extravasation studies. While traditional sealed microfluidic devices allow visualization of specific extravasation processes (56), they cannot often recover extravasated cells efficiently. This limitation prevents downstream analyses for characterizing disseminated cell phenotypic and molecular profiling. Our device introduces a customizable collection chamber, providing a unique advantage: it facilitates the straightforward isolation and collection of extravasated cells without disrupting the experimental setup. This innovation allows researchers to combine dynamic live-imaging capabilities with high-resolution post-extravasation analyses, such as gene expression profiling, functional assays, or single-cell sequencing. Furthermore, incorporating a porous membrane mimics the *in vivo* vascular basement membrane more effectively than many other systems, enhancing the physiological relevance of the model (56). Also, HUVECs have been shown to secrete and deposit key extracellular matrix components, including type IV collagen and laminin, particularly in 3D culture or under specific environmental conditions such as hypoxia (57,58). Forbetter endothelial adherence on PDMS and as HUVEC will be able to secrete their own ECM, we chose to Fibronectin and Type I collagen. Indeed, both are commonly used to coat PDMS/glass microfluidic devices containing HUVECs, particularly in 3D vessel models, as they promote endothelial cell adhesion, spreading, and physiological morphology. Fibronectin exhibits excellent adsorption onto PDMS surfaces, enhancing HUVEC attachment (59–61). Type I collagen, in turn, significantly increases the hydrophilicity of PDMS, supports stable cell adhesion even under flow conditions, and is also widely used in endothelialized vascular models (62,63).

Another key strength lies in its ability to model endothelial functions under shear stress and inflammatory conditions. Unlike static culture systems, the inclusion of shear flow more accurately simulates the hemodynamic environment of blood vessels, leading to a more realistic reconstitution of the extravasation process (64,65). Such functionality is particularly valuable for studying interactions between metastatic cancer cells or immune cells and the endothelial barrier. By enabling real-time visualization coupled with retrieving viable extravasated cells, our device bridges the gap between dynamic imaging and subsequent molecular analyses—a feat rarely achieved by other systems described in the current

literature (66). In this study, we also observed dynamic vascular remodeling events, including local widening of endothelial junctions and the formation of intercellular gaps during metastatic extravasation. While these features were not included in the current figures due, it could be interesting to optimize high-resolution live-imaging strategies to capture and quantify these events more precisely. Our observations are consistent with *in vivo* studies showing that inflammatory cytokines such as TNF-α promote endothelial remodeling through actin cytoskeletal reorganization and junctional destabilization, facilitating tumor cell transendothelial migration (67,68). Moreover, recent intravital imaging analyses have highlighted the active role of endothelial cells in guiding or resisting metastatic cell extravasation, through transient gap formation or endothelial enwrapment (42,69). These results underline the importance of vascular dynamics in metastatic progression, and future versions of our model will aim to integrate these parameters more quantitatively and visually.

Our microfluidic platform holds the potential to significantly advance the field of cancer and immune biology by enabling novel insights into the extravasation process and the characterization of disseminated cells. For instance, by isolating extravasated cells, researchers can identify specific molecular markers or transcriptional programs associated with metastatic potential. This could elucidate why specific cancer cells successfully disseminate while others do not, aiding in developing targeted anti-metastatic therapies. The device could also include co-culture systems within the collection chamber, such as stromal, organ-specific environments, or immune cells. This would enable the study of how interactions between disseminated cancer cells and their new microenvironment drive secondary tumor formation. Also, a limitation of our current setup is the absence of pulsatile flow and physiological viscosity, which may influence cell arrest and adhesion dynamics; future developments will aim to incorporate these parameters to more accurately mimic in vivo hemodynamic conditions.

Beyond cancer studies, the platform could be used to investigate immune cell extravasation during inflammation or immune surveillance. This could provide insights into how immune cells migrate and respond to pathological conditions, with implications for developing therapies for autoimmune diseases or enhancing immune-based cancer treatments (70).This study is the use of a single cancer cell line (MDA-MB-231) and HL-60 cells as immune cell mimics. While sufficient for validating the functionality of the platform, future studies will expand to include additional tumor models with distinct extravasation profiles—such as molecularly modified cell lines or patient-derived CTCs—as well as more physiologically relevant immune cells, in order to dissect the cellular and molecular mechanisms driving extravasation.Also, by incorporating this device into drug screening pipelines, researchers could assess the effects of therapeutic compounds on the extravasation process in real-time. For example, anti-adhesion or anti-invasion drugs could be tested for their ability to inhibit extravasation under flow conditions (71). Collected extravasated cells could be subjected to cutting-edge single-cell multi-omic analyses, providing unparalleled cellular and molecular heterogeneity resolution in disseminated cells. This would pave the way for discovering novel therapeutic targets and understanding resistance mechanisms.

Conclusions

The described microfluidic device addresses critical limitations in the field and opens new avenues for investigating complex biological processes with high translational relevance. Its application is poised to yield breakthroughs in understanding metastasis, immune dynamics, and vascular biology, with significant implications for therapeutic innovation.

Supplementary Material

The supplementary information provides additional validation and technical details supporting the study. It includes confocal and brightfield images showing HUVEC proliferation and organization inside the microfluidic channels under flow, with staining for CD31 and VE-cadherin to confirm endothelial identity and junction formation. Several 3D animation movies illustrate endothelial layer architecture and dynamics, as well as time-lapse recordings of leukocyte (HL-60) and breast cancer (MDA-MB-231) cell interactions with the endothelium during rolling, adhesion, and extravasation. Additional figures report gene expression comparisons between HUVECs and fibroblasts, and between cancer cells and endothelial cells, confirming phenotypic specificity. Further data document MDA-MB-231 extravasation through TNFα-activated endothelium in the presence of CXCL12. Technical aspects are detailed, including mold design files (Autodesk Fusion) for chip fabrication, flow calibration and stability analyses, and confocal image tiling of the collecting chamber. Altogether, these data demonstrate the robustness, reproducibility, and functional validation of the microfluidic platform.

Author contributions

All authors conceived and designed experiments. AS and FW performed most of the research and analyzed the data. JD and MD support cell culture and the first step of microfluidic use. FS performed all gene expression analyses. CL and AT supervised the study and acquired the funding. AS and FW wrote the first draft of the manuscript, and all authors edited it.

Conflicts of interest

There are no conflicts to declare.

Data availability

The materials used during the current study are available from the corresponding author upon reasonable request. Data sharing does not apply to this article, as no datasets were generated or analyzed during the current study.

Acknowledgements

We thank the ONCOLille Institute. This work is supported by a Contrat de Plan Etat-Région CPER Cancer 2015-2020 grant. Chann Lagadec receives a Contrat de Plan Etat-Région CPER Cancer 2015-2020 fellowship. Marie Denoulet was supported by a grant fellowship from The Ligue Contre le Cancer. We would like to thank the cytometry platform of the Bio-Imaging Center of Lille (BICeL) and Sophie Salomé-Desnoulez, in particular, for her help with imaging systems.

Our research is supported by the INCa (French Cancer National Institute), Grant number INCA_9276, by Ligue Contre le Cancer - Septentrion Comity, by the SIRIC ONCOLille, by "Ruban Rose!" charity award, by Institut pour la Recherche sur le Cancer de Lille (IRCL), by Centre Oscar Lambret and by GEFLUC Charity.

References

1. Chaffer CL, Weinberg RA. A Perspective on Cancer Cell Metastasis. Science. 2011 Mar 25;331(6024):1559–64.

2. Arvelo F, Sojo F, Cotte C. Tumour progression and metastasis. ecancer [Internet]. 2016 Jan 29 [cited 2025 Feb 13];10. Available from: http://www.ecancer.org/journal/10/full/617-tumour-progression-and-metastasis.php

3. Fidler IJ. The pathogenesis of cancer metastasis: the "seed and soil" hypothesis revisited. Nat Rev Cancer. 2003 Jun;3(6):453–8.

4. Nguyen DX, Bos PD, Massagué J. Metastasis: from dissemination to organ-specific colonization. Nat Rev Cancer. 2009 Apr;9(4):274–84.

5. Weilbaecher KN, Guise TA, McCauley LK. Cancer to bone: a fatal attraction. Nat Rev Cancer. 2011 Jun;11(6):411–25.

6. Giavazzi R, Foppolo M, Dossi R, Remuzzi A. Rolling and adhesion of human tumor cells on vascular endothelium under physiological flow conditions. J Clin Invest. 1993 Dec 1;92(6):3038–44.

7. Miles FL, Pruitt FL, Van Golen KL, Cooper CR. Stepping out of the flow: capillary extravasation in cancer metastasis. Clin Exp Metastasis. 2008 Jun;25(4):305–24.

8. Shoval H, Karsch-Bluman A, Brill-Karniely Y, Stern T, Zamir G, Hubert A, et al. Tumor cells and their crosstalk with endothelial cells in 3D spheroids. Sci Rep. 2017 Sep 5;7(1):10428.

9. Choi Y, Hyun E, Seo J, Blundell C, Kim HC, Lee E, et al. A microengineered pathophysiological model of early-stage breast cancer. Lab Chip. 2015;15(16):3350–7.

10. Skardal A, Devarasetty M, Kang HW, Mead I, Bishop C, Shupe T, et al. A hydrogel bioink toolkit for mimicking native tissue biochemical and mechanical properties in bioprinted tissue constructs. Acta Biomaterialia. 2015 Oct;25:24–34.

11. Portillo-Lara R, Annabi N. Microengineered cancer-on-a-chip platforms to study the metastatic microenvironment. Lab Chip. 2016;16(21):4063–81.

12. Yanakieva I, Erzberger A, Matejčić M, Modes CD, Norden C. Cell and tissue morphology determine actin-dependent nuclear migration mechanisms in neuroepithelia. Journal of Cell Biology. 2019 Oct 7;218(10):3272–89.

13. Wrighton PJ, Shwartz A, Heo JM, Quenzer ED, LaBella KA, Harper JW, et al. Quantitative intravital imaging in zebrafish reveals in vivo dynamics of physiological-stress-induced mitophagy. J Cell Sci. 2021 Feb 22;134(4):jcs256255.

14. Follain G, Osmani N, Azevedo AS, Allio G, Mercier L, Karreman MA, et al. Hemodynamic Forces Tune the Arrest, Adhesion, and Extravasation of Circulating Tumor Cells. Developmental Cell. 2018 Apr;45(1):33-52.e12.

15. Bernardello M, Marsal M, Gualda EJ, Loza-Alvarez P. Light-sheet fluorescence microscopy for the in vivo study of microtubule dynamics in the zebrafish embryo. Biomed Opt Express, BOE. 2021 Oct 1;12(10):6237–54.

16. Kienast Y, von Baumgarten L, Fuhrmann M, Klinkert WEF, Goldbrunner R, Herms J, et al. Real-time imaging reveals the single steps of brain metastasis formation. Nat Med. 2010 Jan;16(1):116–22.

17. Arvanitis CD, Ferraro GB, Jain RK. The blood–brain barrier and blood–tumour barrier in brain tumours and metastases. Nat Rev Cancer. 2020 Jan;20(1):26–41.

18. Peralta M, Dupas A, Larnicol A, Lefebvre O, Goswami R, Stemmelen T, et al. Endothelial calcium firing mediates the extravasation of metastatic tumor cells. iScience [Internet]. 2025 Feb 21 [cited 2025 Aug 7];28(2). Available from: https://www.cell.com/iscience/abstract/S2589-0042(24)02917-1

19. Costa-Silva B, Aiello NM, Ocean AJ, Singh S, Zhang H, Thakur BK, et al. Pancreatic cancer exosomes initiate pre-metastatic niche formation in the liver. Nat Cell Biol. 2015 Jun;17(6):816–26.

20. Schoumacher M, Goldman RD, Louvard D, Vignjevic DM. Actin, microtubules, and vimentin intermediate filaments cooperate for elongation of invadopodia. J Cell Biol. 2010 May 3;189(3):541–56.

21. Eddy RJ, Weidmann MD, Sharma VP, Condeelis JS. Tumor Cell Invadopodia: Invasive Protrusions that Orchestrate Metastasis. Trends Cell Biol. 2017 Aug;27(8):595–607.

22. Clark AG, Vignjevic DM. Modes of cancer cell invasion and the role of the microenvironment. Curr Opin Cell Biol. 2015 Oct;36:13–22.

23. Lu X, Mu E, Wei Y, Riethdorf S, Yang Q, Yuan M, et al. VCAM-1 promotes osteolytic expansion of indolent bone micrometastasis of breast cancer by engaging α4β1-positive osteoclast progenitors. Cancer Cell. 2011 Dec 13;20(6):701–14.

24. Targeting S100A9–ALDH1A1–Retinoic Acid Signaling to Suppress Brain Relapse in EGFR-Mutant Lung Cancer | Cancer Discovery | American Association for Cancer Research [Internet]. [cited 2025 Aug 7]. Available from: https://aacrjournals-org.proxy.insermbiblio.inist.fr/cancerdiscovery/article/12/4/1002/689611/Targeting-S100A9-ALDH1A1-Retinoic-Acid-Signaling

25. Figuerêdo SH, Neto RSC, Ferreira E, Cassali GD, Estrela-Lima A, Damasceno KA. Expression of VCAN and its receptors in canine mammary carcinomas with or without myoepithelial proliferation. Res Vet Sci. 2021 Nov;140:56–63.

26. Entenberg D, Oktay MH, Condeelis JS. Intravital imaging to study cancer progression and metastasis. Nat Rev Cancer. 2023 Jan;23(1):25–42.

27. Bhatia SN, Ingber DE. Microfluidic organs-on-chips. Nat Biotechnol. 2014 Aug;32(8):760–72.

28. Wells CM, Parsons M, editors. Cell Migration: Developmental Methods and Protocols [Internet]. Totowa, NJ: Humana Press; 2011 [cited 2024 Mar 1]. (Methods in Molecular Biology; vol. 769). Available from: https://link.springer.com/10.1007/978-1-61779-207-6

29. Song JW, Cavnar SP, Walker AC, Luker KE, Gupta M, Tung YC, et al. Microfluidic Endothelium for Studying the Intravascular Adhesion of Metastatic Breast Cancer Cells. Blagosklonny MV, editor. PLoS ONE. 2009 Jun 1;4(6):e5756.

30. Zervantonakis IK, Hughes-Alford SK, Charest JL, Condeelis JS, Gertler FB, Kamm RD. Three-dimensional microfluidic model for tumor cell intravasation and endothelial barrier function. Proc Natl Acad Sci USA. 2012 Aug 21;109(34):13515–20.

31. Jeon JS, Bersini S, Gilardi M, Dubini G, Charest JL, Moretti M, et al. Human 3D vascularized organotypic microfluidic assays to study breast cancer cell extravasation. Proc Natl Acad Sci USA. 2015 Jan 6;112(1):214–9.

32. Kühlbach C, da Luz S, Baganz F, Hass V, Mueller M. A Microfluidic System for the Investigation of Tumor Cell Extravasation. Bioengineering. 2018 May 23;5(2):40.

33. Wu Y, Zhou Y, Paul R, Qin X, Islam K, Liu Y. Adaptable Microfluidic Vessel-on-a-Chip Platform for Investigating Tumor Metastatic Transport in Bloodstream. Anal Chem. 2022 Sep 6;94(35):12159–66.

34. Hajal C, Shin Y, Li L, Serrano JC, Jacks T, Kamm RD. The CCL2-CCR2 astrocyte-cancer cell axis in tumor extravasation at the brain. Sci Adv. 2021 Jun 25;7(26):eabg8139.

35. Liu W, Song J, Du X, Zhou Y, Li Y, Li R, et al. AKR1B10 (Aldo-keto reductase family 1 B10) promotes brain metastasis of lung cancer cells in a multi-organ microfluidic chip model. Acta Biomaterialia. 2019 Jun;91:195–208.

36. Lagadec C, Meignan S, Adriaenssens E, Foveau B, Vanhecke E, Romon R, et al. TrkA overexpression enhances growth and metastasis of breast cancer cells. Oncogene. 2009 May 7;28(18):1960–70.

37. Delannoy E, Tellier G, Cholet J, Leroy AM, Treizebré A, Soncin F. Multi-Layered Human Blood Vessels-on-Chip Design Using Double Viscous Finger Patterning. Biomedicines. 2022 Mar 29;10(4):797.

38. Livak KJ, Schmittgen TD. Analysis of relative gene expression data using real-time quantitative PCR and the 2(-Delta Delta C(T)) Method. Methods. 2001 Dec;25(4):402–8.

39. Huynh PD, Van Pham P, Vu NB. Exosomes Derived from Human Umbilical Cord Mesenchymal Stem Cells Enhance Angiogenesis Through Upregulation of the VWF and Flk1 Genes in Endothelial Cells. Adv Exp Med Biol. 2023 Apr 5;

40. Sarabipour S, Kinghorn K, Quigley KM, Kovacs-Kasa A, Annex BH, Bautch VL, et al. Trafficking dynamics of VEGFR1, VEGFR2, and NRP1 in human endothelial cells. PLoS Comput Biol. 2024 Feb;20(2):e1011798.

41. Carman CV, Springer TA. A transmigratory cup in leukocyte diapedesis both through individual vascular endothelial cells and between them. J Cell Biol. 2004 Oct 25;167(2):377–88.

42. Reymond N, d'Água BB, Ridley AJ. Crossing the endothelial barrier during metastasis. Nat Rev Cancer. 2013 Dec;13(12):858–70.

43. DeMaio L, Tseng W, Balverde Z, Alvarez JR, Kim KJ, Kelley DG, et al. Characterization of mouse alveolar epithelial cell monolayers. American Journal of Physiology-Lung Cellular and Molecular Physiology. 2009 Jun;296(6):L1051–8.

44. Chen MB, Whisler JA, Jeon JS, Kamm RD. Mechanisms of tumor cell extravasation in an in vitro microvascular network platform. Integr Biol. 2013;5(10):1262.

45. Waite L, Fine JM. Applied biofluid mechanics. New York: McGraw-Hill; 2007. 1 p.

46. Wang X, Lee J, Ali M, Kim J, Lacerda CMR. Phenotype Transformation of Aortic Valve Interstitial Cells Due to Applied Shear Stresses Within a Microfluidic Chip. Ann Biomed Eng. 2017 Oct;45(10):2269–80.

47. Tsao CW, Cheng YC, Cheng JH. Fluid Flow Shear Stress Stimulation on a Multiplex Microfluidic Device for Rat Bone Marrow Stromal Cell Differentiation Enhancement. Micromachines. 2015 Dec 11;6(12):1996–2009.

48. Tsao CW, Yeh LC, Cheng YC. Mechanical-stress microfluidic device for stem cell stimulation. In: 2014 IEEE International Nanoelectronics Conference (INEC) [Internet]. Sapporo, Japan: IEEE; 2014 [cited 2024 Jul 22]. p. 1–2. Available from: http://ieeexplore.ieee.org/document/7460332/

49. Dekker RJ, Van Soest S, Fontijn RD, Salamanca S, De Groot PG, VanBavel E, et al. Prolonged fluid shear stress induces a distinct set of endothelial cell genes, most specifically lung Krüppel-like factor (KLF2). Blood. 2002 Sep 1;100(5):1689–98.

50. Luo JY, Cheng CK, He L, Pu Y, Zhang Y, Lin X, et al. Endothelial UCP2 Is a Mechanosensitive Suppressor of Atherosclerosis. Circulation Research. 2022 Aug 19;131(5):424–41.

51. Magder S, Neculcea J, Neculcea V, Sladek R. Lipopolysaccharide and TNF-α Produce Very Similar Changes in Gene Expression in Human Endothelial Cells. J Vasc Res. 2006;43(5):447–61.

52. Viemann D, Goebeler M, Schmid S, Klimmek K, Sorg C, Ludwig S, et al. Transcriptional profiling of IKK2/NF-κB— and p38 MAP kinasedependent gene expression in TNF-α—stimulated primary human endothelial cells. Blood. 2004 May 1;103(9):3365–73.

53. Murakami T, Mataki C, Nagao C, Umetani M, Wada Y, Ishii M, et al. The Gene Expression Profile of Human Umbilical Vein Endothelial Cells Stimulated by Tumor Necrosis Factor a Using DNA Microarray Analysis. J Atheroscler Thromb. 2000;7(1):39–44.

54. Riahi R, Yang YL, Kim H, Jiang L, Wong PK, Zohar Y. A microfluidic model for organ-specific extravasation of circulating tumor cells. Biomicrofluidics. 2014 Mar 1;8(2):024103.

55. Ellinghaus P, Perzborn E, Hauenschild P, Gerdes C, Heitmeier S, Visser M, et al. Expression of pro-inflammatory genes in human endothelial cells: Comparison of rivaroxaban and dabigatran. Thrombosis Research. 2016 Jun;142:44–51.

56. García-Chamé M, Wadhwani P, Pfeifer J, Schepers U, Niemeyer CM, Domínguez CM. A Versatile Microfluidic Platform for Extravasation Studies Based on DNA Origami—Cell Interactions. Angew Chem Int Ed. 2024 Jul 8;63(28):e202318805.

57. Kusuma S, Zhao S, Gerecht S. The extracellular matrix is a novel attribute of endothelial progenitors and of hypoxic mature endothelial cells. FASEB J. 2012 Dec;26(12):4925–36.

58. Zeitouni S, Krause U, Clough BH, Halderman H, Falster A, Blalock DT, et al. Human Mesenchymal Stem Cell–Derived Matrices for Enhanced Osteoregeneration. Science Translational Medicine. 2012 May 2;4(132):132ra55-132ra55.

59. Chumbimuni-Torres KY, Coronado RE, Mfuh AM, Castro-Guerrero C, Silva MF, Negrete GR, et al. Adsorption of Proteins to Thin-Films of PDMS and Its Effect on the Adhesion of Human Endothelial Cells. RSC Adv. 2011 Sep 21;1(4):706–14.

60. Cornelissen CG, Dietrich M, Gromann K, Frese J, Krueger S, Sachweh JS, et al. Fibronectin coating of oxygenator membranes enhances endothelial cell attachment. BioMedical Engineering OnLine. 2013 Jan 28;12(1):7.

61. Spuul P, Chi PY, Billottet C, Chou CF, Génot E. Microfluidic devices for the study of actin cytoskeleton in constricted environments: Evidence for podosome formation in endothelial cells exposed to a confined slit. Methods. 2016 Feb 1;94:65–74.

62. Siddique A, Meckel T, Stark RW, Narayan S. Improved cell adhesion under shear stress in PDMS microfluidic devices. Colloids and Surfaces B: Biointerfaces. 2017 Feb 1;150:456–64.

63. Sivarapatna A, Ghaedi M, Xiao Y, Han E, Aryal B, Zhou J, et al. Engineered Microvasculature in PDMS Networks Using Endothelial Cells Derived from Human Induced Pluripotent Stem Cells. Cell Transplant. 2017 Aug;26(8):1365–79.

64. Li YSJ, Haga JH, Chien S. Molecular basis of the effects of shear stress on vascular endothelial cells. Journal of Biomechanics. 2005 Oct;38(10):1949–71.

65. Tsaryk R, Yucel N, Leonard EV, Diaz N, Bondareva O, Odenthal-Schnittler M, et al. Shear stress switches the association of endothelial enhancers from ETV/ETS to KLF transcription factor binding sites. Sci Rep. 2022 Mar 21;12(1):4795.

66. Zhang X, Karim M, Hasan MM, Hooper J, Wahab R, Roy S, et al. Cancer-on-a-Chip: Models for Studying Metastasis. Cancers. 2022 Jan 27;14(3):648.

67. Shivanna M, Srinivas SP. Elevated cAMP opposes (TNF-α)-induced loss in the barrier integrity of corneal endothelium. Mol Vis. 2010 Sep 2;16:1781–90.

68. Angelini DJ, Hyun SW, Grigoryev DN, Garg P, Gong P, Singh IS, et al. TNF-α increases tyrosine phosphorylation of vascular endothelial cadherin and opens the paracellular pathway through fyn activation in human lung endothelia. American Journal of Physiology-Lung Cellular and Molecular Physiology. 2006 Dec;291(6):L1232–45.

69. Follain G, Osmani N, Gensbittel V, Asokan N, Larnicol A, Mercier L, et al. Impairing flow-mediated endothelial remodeling reduces extravasation of tumor cells. Sci Rep. 2021 Jun 23;11(1):13144.

70. Boussommier-Calleja A, Li R, Chen MB, Wong SC, Kamm RD. Microfluidics: A New Tool for Modeling Cancer–Immune Interactions. Trends in Cancer. 2016 Jan;2(1):6–19.

71. Kim C, Kasuya J, Jeon J, Chung S, Kamm RD. A quantitative microfluidic angiogenesis screen for studying anti-angiogenic therapeutic drugs. Lab Chip. 2015;15(1):301–10.